Research Square

Preprints are preliminary reports that have not undergone peer review.
They should not be considered conclusive, used to inform clinical practice,
or referenced by the media as validated information.

Initial transcriptomic reprogramming reveals distinct dose-dependent responses of Microcystis aeruginosa to polyaluminum chloride

Eun-jeong Kim

kim2@cau.ac.kr

Chung-Ang University https://orcid.org/0000-0003-3322-9314

Research Article

Keywords: Microcystis bloom; RNA sequencing; Polyaluminum chloride; Photosystem II; Bacterial secretion system; Toxin–antitoxin system

Posted Date: November 19th, 2026

DOI: https://doi.org/10.21203/rs.3.rs-11778906/v1

License: This work is licensed under a Creative Commons Attribution 4.0 International License.
Read Full License

Additional Declarations: The authors declare no competing interests.

[Research Article] Running Head: *Microcystis* to PAC exposure

Initial transcriptomic reprogramming reveals distinct dose-dependent responses of *Microcystis aeruginosa* to polyaluminum chloride

Yeon-jeong Park[1], Jae Hak Lee[2], Heesuk Lee[1], Han Soon Kim[3], Eun-jeong Kim[4*]

[1]Water environmental Management Department, Korea Water Resources Corporation, Daejeon 34350, Korea

[2]Freshwater Bioresources Culture Collection (FBCC), Nakdonggang National Institute of Biological Resources, Sangju 37242, Korea

[3]Department of Life Science, Kyungpook National University, Daegu 41566, Korea

[4]Department of Life Science, Chung-Ang University, Seoul 06974, Korea

* Corresponding author.

E-mail address: kim2@cau.ac.kr (E. Kim).

Yeon-jeong Park (orcid ID: 0000-0003-3817-8341)

Jae Hak Lee (orcid ID: 0000-0001-5016-6496)

Heesuk Lee (orcid ID: 0000-0002-3632-7692)

Han Soon Kim (orcid ID: 0000-0002-8186-3849)

Eun-jeong Kim (orcid ID: 0000-0003-3322-9314)

Preprint not peer reviewed

This preprint research paper has not been peer reviewed. Electronic copy available at: https://ssrn.com/abstract=7398765

Highlights

- PAC exposure induced rapid transcriptomic reprogramming in *Microcystis aeruginosa*.
- Low PAC exposure caused minor growth inhibition and increased expression of bacterial secretion system genes.
- PAC stress altered expression of phycobilisome-related genes and reduced phycocyanin production.
- High PAC exposure increased expression of toxin–antitoxin system genes.
- PAC exposure revealed bacterial defense mechanisms as key components of chemical stress responses.

Preprint not peer reviewed

This preprint research paper has not been peer reviewed. Electronic copy available at: https://ssrn.com/abstract=7398765

Abstract

Polyaluminum chloride (PAC) is widely used as a coagulant to facilitate the removal of dense cyanobacterial scum in eutrophic lakes. Although PAC effectively removes bloom biomass through coagulation, not all PAC-exposed cells are incorporated into flocs. The remaining suspended cells may survive and rapidly recover under elevated temperature conditions. Therefore, we aimed to characterize the early transcriptional responses of *M. aeruginosa* to PAC exposure and identify molecular pathways associated with cellular persistence and recovery. To address this research gap, we investigated growth, photosynthetic pigments, and transcriptomic responses of *M. aeruginosa* under low (40 ppm) and high (400 ppm) PAC exposure, including a time-course analysis of the low treatment. Following low PAC treatment, cell density decreased by approximately 10% after 24 h, whereas overall growth patterns remained similar to those of the untreated control. Time-course RNA sequencing under low PAC exposure identified 264 unique differentially expressed genes across the 3 h, 6 h, and 24 h sampling points, including genes associate with bacterial secretion system and photosynthetic processes. Genes involved in photosystem II antenna complexes and phycobilisome were downregulated at 3 h after PAC exposure, preceding a decline in phycocyanin (PC) content. Under high PAC exposure, 302 genes were differentially expressed within 3 h, including multiple type II toxin–antitoxin system genes associated with cellular stress responses. These findings reveal dynamic early response strategies in cyanobacteria under chemical stress, providing a framework for understanding the processes responsible for adaptation and survival under environmental perturbations and informing future bloom management strategies.

Keywords

Microcystis bloom; RNA sequencing; Polyaluminum chloride; Photosystem II; Bacterial secretion system; Toxin–antitoxin system

Preprint not peer reviewed

This preprint research paper has not been peer reviewed. Electronic copy available at: https://ssrn.com/abstract=7398765

1. Introduction

In recent decades, harmful cyanobacterial blooms have become more frequent, intense, and persistent due to the combined effects of eutrophication and climate change (Miranda et al. 2017, Glibert 2020, Yang et al. 2024). During summer, extensive blooms of *Microcystis* and other cyanobacterial genera can threaten drinking water supplies and recreational activities (Yan et al. 2017, Wilhelm Steven et al. 2020, Kim et al. 2024).

The removal of cyanobacterial biomass and surface scums is a key objective of bloom management, and various chemical and physical approaches have been developed to improve removal efficiency (Ndikubwimana et al. 2016, Zhang et al. 2019). Chemical treatments applied for cyanobacterial bloom control commonly alter fundamental cellular processes, including photosynthesis, membrane function, and stress-response pathways, thereby influencing the physiological state of exposed cells (Hong et al. 2009, Zhang et al. 2023). Despite these insights, most studies have focused on bloom control and growth inhibition, with little attention given to the mechanisms enabling the survival of chemically exposed cells. Understanding their molecular processes is essential for elucidating the biological strategies that promote persistence and subsequent bloom recovery.

Polyaluminum chloride (PAC) is widely used as a coagulant in water treatment and has been applied for cyanobacterial bloom mitigation in eutrophic waters (EPA 2022). Previous studies have primarily focused on coagulation efficiency and biomass removal (Lürling et al. 2020, Arruda et al. 2021, Zhang et al. 2022). However, the effectiveness of PAC treatments also varies with environmental conditions. For example, cyanobacterial populations from Lake de Kuil rapidly resurfaced after PAC-based coagulation treatment, whereas more persistent removal was achieved in Lake Rauwbraken under similar conditions, highlighting the influence of site-specific factors on treatment efficacy (Lürling et al. 2020). These observations suggest that a fraction of PAC-treated cells may remain viable despite substantial biomass reduction, providing a potential source for bloom recovery favorable environmental conditions. Therefore, characterizing the cellular responses of PAC-exposed cells may provide critical insights into the biological processes underlying survival, adaptation, and subsequent bloom recovery. Comparing these responses with later physiological outcomes could help establish a mechanistic framework for improving the long-term effectiveness of cyanobacterial bloom management strategies.

Preprint not peer reviewed

This preprint research paper has not been peer reviewed. Electronic copy available at: https://ssrn.com/abstract=7398765

Environmental stress often induces rapid transcriptional reprogramming that precedes and ultimately influences cellular physiology and adaptation (Casamassimi and Ciccodicola 2019). RNA-seq enables the simultaneous characterization of genes and biological pathways, allowing both established and previously unrecognized components of cellular stress responses to be identified (Wang et al. 2009, Stark et al. 2019). In cyanobacteria, transcriptomic studies have revealed common responses to diverse environmental challenges, including the reorganization of photosynthesis, membrane transport, metabolism, and general stress-response pathways (Sinetova and Los 2016, Yang et al. 2020). Studies of *Microcystis* have further demonstrated coordinated gene-expression changes under different nutrient conditions, microbial interactions, and chemical stress, thereby providing insights into regulatory networks associated with stress adaptation and environmental persistence (Harke et al. 2012, Harke and Gobler 2015, Morimoto et al. 2018, Yang et al. 2020, Yang et al. 2022, Du et al. 2023, Ma et al. 2023). Nevertheless, the transcriptional responses and regulatory pathways triggered by PAC exposure in *Microcystis* remain largely unexplored. Field transcriptomic surveys offer valuable ecological relevance, yet the simultaneous influence of temperature, nutrient availability, community composition, and other environmental variables often complicates attribution to a single stressor (Harke and Gobler 2013, Tang et al. 2018, Lürling et al. 2020). Therefore, controlled RNA-seq experiments can distinguish PAC-specific transcriptional response and clarify the biological strategies underlying cellular adaptation.

To address this research gap, we employed RNA-seq to characterize the transcriptomic responses of *Microcystis* to PAC exposure. We further examined growth, photosynthetic pigments, and transcriptomic responses under low and high PAC exposure, including time-course analyses under low PAC conditions. This study provides a framework for understanding cyanobacterial adaptation to chemical stress and may improve predictions of bloom persistence under chemical treatment.

Preprint not peer reviewed

This preprint research paper has not been peer reviewed. Electronic copy available at: https://ssrn.com/abstract=7398765

2. Materials and methods

2.1. Culture conditions and frozen cells

The *M. aeruginosa* strain KW (KCTC 18162P) was obtained from the Korean Collection for Type Cultures (Jeong et al. 2018). This strain was grown axenically in a 500 ml flask containing 300 ml of BG-11 medium (Fig. 1). The cells were cultured under a light intensity of 30 ± 1 μmol m^{-2} s^{-1} at 25°C on a shaker. The strain was precultured for one week and collected using centrifugation at 4000 rpm for 5 min. The cells were washed three times with fresh BG-11 and then resuspended in the same medium. The cells were reinoculated at a density of 6 × 10^6 cells/mL into both a 40 ppm or 400 ppm PAC solution, representing concentrations commonly used in water treatment, and severe chemical stress, respectively (Najm et al. 1998, Mehdizadeh et al. 2020). After incubation, each sample was washed and centrifuged, and the supernatant was removed. The pellets were immediately frozen in liquid nitrogen and stored in a freezer at –70°C. RNA isolation was conducted within one week, and RNA-seq analysis was performed using a single dataset at three points: 3 h, 6 h, and 24 h. Under high PAC treatment, the total RNA concentration was insufficient for RNA-seq at 6 h and 24 h, possibly due to RNA degradation caused by PAC-induced damage.

2.2. PAC solutions

PAC are commonly applied in primary coagulation in drinking water and municipal wastewater treatment (Najm et al. 1998, Mehdizadeh et al. 2020). Microalgae in water exist in a colloidal state and move due to electrostatic repulsion. Adding a coagulant with an opposite charge induces flocculation (Kurniawan et al. 2022). Consequently, microalgal scum can be effectively removed in water treatment processes, making this method useful for addressing seasonal microalgal blooms. In this study, two flasks were treated with PAC at concentration of 40 mg/L and 400 mg/L, with no pH adjustment. The stock PAC solution was prepared in distilled water and stored at room temperature.

2.3. Growth curves and doubling time calculation

Preprint not peer reviewed

This preprint research paper has not been peer reviewed. Electronic copy available at: https://ssrn.com/abstract=7398765

Three flasks, representing no treatment, low PAC treatment, and high PAC treatment, were cultured in triplicate. From each sample, 1mL was collected at 3 h, 6 h, and 24 h, as well as 1 d, 2 d, 3 d, and 8 d for cell counting (Fig. 2A). This study used *M. aeruginosa* KW, a stain that lost its colony-forming ability due to a long-term culture after being isolated in 2008 (BioSample: SAMN06339528). Upon PAC exposure, individual cells settled at the bottom instead of forming aggregates. Following incubation on a shaker, these samples were stained with Lugol's iodine, and the cells were counted using a Hemocytometer C-Chip (NCYTO®), with the counts repeated 15 times. The average cell number was used for growth curve analysis (Fig. 2A). The specific growth rate (μ), also called the growth rate constant, describes the rate of exponential growth per unit time and is calculated as $\mu = ((\ln (N_t / N_0)) / t$, where N_t is the population size at time t, N_0 is the initial population size, and t is the time interval (h). The doubling time (t*d*) was calculated using the equation t*d*=ln(2)/μ. Based on the estimated growth rates, t*d* was 90.0 h (3.75 days) for the control [ln(2)/0.0077] and 101.9 h (4.25 days) for the 40 ppm PAC treatment [ln(2)/0.0068] (Table S1). In addition, microscopic images were taken to observe phenotypic changes, including pigment fading and cell wall disruption (Fig. 2B).

2.4. Photosynthetic pigment content

Following incubation for 3 h, 6 h, and 24 h, as well as 1 d, 2 d, and 3 d, with three biological replicates for each time point (Fig. 2C - E), samples were centrifuged at 4,000 rpm for 10 min, and the pellets were extracted with 1 mL of 90% acetone. Chlorophyll-*a* concentrations were determined by measuring the optical density at 750, 663, 645, and 630 nm, using 90% acetone as the blank (Rice et al. 2012). Phycocyanin was extracted for four freeze-thaw cycles consisting of freezing at –20℃ and thawing at room temperature, following by measurement of the optical density at 615 and 652 nm (Bennett and Bogorad 1973). All photosynthetic pigments were quantified using a spectrophotometer (Fig. 2D and 2E). In addition, pH was measured (Fig. 2C).

2. 5. Illumina sequencing and transcriptome analysis

Preprint not peer reviewed

This preprint research paper has not been peer reviewed. Electronic copy available at: https://ssrn.com/abstract=7398765

The frozen pellets from Section 2.1 were used for total RNA isolation using a Maxwell 16-cell LEV RNA purification kit for plants, following the manufacturer's instructions (Promega). The library was prepared according to Illumina's specifications. The quality and integrity of the RNA were determined using an Agilent Technologies 2100 Bioanalyzer (Agilent, Germany). The samples were sequenced on an Illumina NovaSeq 6000 Platform, and the clean reads were mapped to *M. aeruginosa* KW as a reference genome (Jeong et al. 2018). Table S2 summarized the RNA-seq sequencing and mapping statistics for each sample, including raw reads, trimmed reads after quality control, filtered reads, and mapping rates to the reference genome.

Differential expression analysis was performed using HTSeq to identify differentially expressed genes (DEGs) between the treatment and control groups. For the temporal analysis of the low PAC treatment, only genes detected in at least two samples of the three sampling time points (3, 6, and 24 h) were retained for downstream analyses. In contrast, differential expression in the high PAC was determined from the single 3 h dataset using the same statistical criteria ($|\log_2 FC| \geq 1$ and a false discovery rate (FDR)-adjusted p-value < 0.05). Gene expression patterns across the 3 h, 6 h, and 24 h time points were analyzed using *k*-means clustering to identify genes with similar expression profiles (MacQueen 1967) (Fig. S3). Clusters of orthologous groups (COGs) classify proteins into functional categories based on their predicted biological roles, facilitating the interpretation of gene functions and biological processes (Galperin et al. 2015, Kang et al. 2024). A hypergeometric test was used to determine whether differentially expressed genes (DEGs) were significantly enriched in Kyoto Encyclopedia of Genes and Genomes (KEGG) pathways. Gene enrichment analysis was performed using the online tool ShinyGO 0.80 with *M. aeruginosa* NIES-843 as the reference organism (http://bioinformatics.sdstate.edu/go/). The ggplot2 package into RStudio was used to generate volcano plots, Venn diagrams, and KEGG enrichment visualizations.

Preprint not peer reviewed

This preprint research paper has not been peer reviewed. Electronic copy available at: https://ssrn.com/abstract=7398765

3. Results

3.1 Physiological responses of Microcystis aeruginosa to PAC exposure

After 8 days of PAC exposure, the *Microcystis* cell densities in the control, low PAC, and high PAC treatment groups were 3.2×10^6 cell mL^{-1}, 2.6×10^6 cell mL^{-1}, and 0.08×10^6 cell mL^{-1}, respectively (Fig. 2A), representing reductions of 18.75% and 97.5% in the low and high PAC exposure, compared to the control. Cell density in high PAC remained relatively stable during the first 3 days but declined sharply thereafter, whereas low PAC maintained a typical growth pattern. Based on the growth curves, the doubling times were estimated to be 3.75 and 4.25 days for the control and low PAC, respectively. Under high PAC exposure, cells appeared enlarged within 3 h and exhibited altered pigmentation with increased intracellular dark granules. These morphological changes became progressively more pronounced, leading to distorted morphology, surface deformation, and visible cellular damage after 3 days (Fig. 2B). Thus, morphological alterations were evident within 3 h, preceding the marked decline in cell density observed after 3 days. In contrast, cells in low PAC remained morphologically similar to those in the control throughout the observation period. The pH remained markedly lower in high PAC throughout the experiment, whereas the control and low PAC maintained similar pH values (Fig. 2C). Chlorophyll-*a* (Chl-*a*) and phycocyanin (PC) generally followed the growth patterns observed in each treatment, although the decline in PC was considerably greater than that of Chl-*a*, particularly under high PAC (Fig. 2D, E). After 3 days, the PC concentration decreased by 11.9% (1.11×10^2 mg m^{-3}) and 88.1% (8.21×10^2 mg m^{-3}) in low and high PAC, respectively, compared with the control.

3.2 Temporal transcriptional responses to low PAC exposure

The early morphological changes observed within 3 h suggested that cellular responses were initiated before measurable growth inhibition (Fig. 2). To characterize these early responses at the molecular level, RNA-seq was performed after 3, 6, and 24 h of low PAC exposure. A heatmap, volcano plots, and a Venn diagram were used to summarize the temporal patterns of DEGs under low PAC exposure (Fig S2). A total of 358 DEGs were identified across the

Preprint not peer reviewed

This preprint research paper has not been peer reviewed. Electronic copy available at: https://ssrn.com/abstract=7398765

three time points (Fig. S2A). The number of upregulated genes was highest at 3 h (111 genes) and decreased to 38 genes at 24 h, whereas downregulated genes increased from 23 genes at 3 h to 90 genes at 24 h (Fig. S2B). Overall, 264 unique DEGs were identified across the three time points (Fig. S2C).

The predominance of upregulated genes at 3 h and the progressive increase in downregulated genes over time suggested distinct temporal transcriptional responses to low PAC exposure. To further characterize these expression patterns, we performed *k*-means clustering of the DEGs (Fig. 3). Approximately half of the 264 unique DEGs were excluded from the clustering analysis because they were annotated as hypothetical proteins, pseudogenes or proteins with domains of unknown function. The 132 functionally annotated DEGs were initially classified into nine clusters (A-I) using *k*-means clustering (Fig. S3). 111 genes (84%) were assigned to the four major clusters (A-D), which are presented in Figure 3A. Cluster A, which contained the largest number of gene (53 genes), showed a transient increase in expression during the early stages of low PAC exposure, followed by a gradual decline at later time points (Fig. 3A). Cluster D (28 genes) exhibited a similar overall declined but showed only a modest increase in expression at 6 h. In contrast, Cluster B and C displayed relatively minor changes in gene expression over time. Because of Cluster A and D represented the predominant temporal expression patterns, KEGG enrichment analysis was performed for these two clusters using and FDR threshold of < 0.05. The eight most significantly enriched pathways in each cluster are shown in Figure 3B. Cluster A was primarily enriched for fatty acid biosynthesis, bacterial secretion system, and signaling pathways, whereas Cluster D was predominantly enriched for photosynthesis-related pathways, including photosynthetic antenna proteins, electron transport, photosynthesis, and thylakoid membrane functions (Fig. 3B).

To further characterize the functional composition of the temporally regulated genes, the 264 DEGs included in the temporal clusters were classified according to the COG database (Fig. S4). The largest numbers of DEGs were assigned to energy production and conversion (category C) and defense mechanisms (category V), indicating that temporal transcriptional responses to low PAC exposure were prominently associated with cellular energy metabolism and defense-related functions. These functional patterns were generally consistent with the metabolic and stress-responsive pathways identified by KEGG pathway analysis.

Preprint not peer reviewed

This preprint research paper has not been peer reviewed. Electronic copy available at: https://ssrn.com/abstract=7398765

3.3 Cluster-specific KEGG pathway enrichment under low PAC exposure

Based on the clustering and KEGG enrichment analyses, representative pathways from the two major expression clusters were mapped onto KEGG pathway diagrams to visualize the distribution of differentially expressed genes within their functional context (Fig. 4).

In Cluster A, differentially expressed genes were predominantly mapped to membrane-associated components of the bacterial secretion system (Fig. 4A). In particular, genes encoding the type I secretion protein HlyD and HlyB were transiently upregulated at 3 h, whereas only a single type II secretion system gene (GspH) exhibited a similar expression pattern. Several genes involved in fatty acid biosynthesis also showed transient induction and were co-clustered with the secretion system genes.

In contrast, genes enriched in Cluster D were broadly distributed across photosynthetic pathways (Fig. 4B). Multiple components of photosystem I (PS I), photosystem II (PS II), photosynthetic electron transport, and photosynthetic antenna proteins were coordinately downregulated during prolonged PAC exposure, indicating progressive suppression of the photosynthetic machinery. The widespread distribution of downregulated genes across the photosynthetic pathway suggests that PAC affected multiple functional components of the photosynthetic apparatus rather than a single photosynthetic complex.

3.4. Comparative transcriptomic responses to high PAC exposure

To compare the early transcriptional responses under severe chemical stress with those observed under low PAC exposure, RNA sequencing was performed on *M. aeruginosa* cells exposed to high PAC for 3 h. Because severe growth inhibition and morphological damage were evident under high PAC, only the 3 h time point was analyzed to capture the initial transcriptional response. Differentially expressed genes (DEGs) were identified using the same criteria as those applied for the low PAC (Fig. 5).

Of the 302 genes differentially expressed under high PAC exposure, 223 were uniquely responsive to 400 ppm PAC and were not differentially expressed under low PAC exposure (Fig. 5A), indicating that increasing PAC concentration triggered a distinct transcriptional program rather than simply amplifying the response observed under low PAC

Preprint not peer reviewed

This preprint research paper has not been peer reviewed. Electronic copy available at: https://ssrn.com/abstract=7398765

conditions. Consistent with this, differential express analysis identified substantially more upregulated gene (183) than downregulated genes (119) under high PAC exposure (Fig. 5B).

To further characterize the functional responses associated with high PAC exposure, KEGG enrichment and Clusters of Orthologous Groups (COGs) functional classification were performed using the 302 differentially expressed genes. KEGG enrichment analysis indicated that upregulated genes were primarily associated with putative transposase, ribonuclease Z/hydroxyacylglutathione hydrolase (Z/HAGH)-like proteins, and enoyl-(acyl carrier protein) reductase, whereas downregulated genes were enriched in photosynthesis-, chlorophyll biosynthesis-, cell wall organization-, and membrane transport-related functions (Fig. 5C). These findings indicate that high PAC exposure is associated with the suppression of photosynthetic and cell envelope-associated functions, together with the activation of genome mobility-related processes. COG classification further supported these findings (Fig. 5D). C (energy production and conversion) and M (cell wall/membrane/envelope biogenesis) contained more than 5-fold as many downregulated genes as upregulated genes, reflecting the suppression of photosynthesis- and cell envelope-associated functions. Conversely, mobilome-related functions (X) showed the greatest increase among the upregulated genes and were uniquely represented, reflecting with the enrichment of transposase-associated genes. O (post-translational modification, protein turnover and chaperones) and V (defense mechanisms) were the next most represented upregulated functional classes, with more than 2.5-fold higher than among downregulated genes. Interestingly, the prominent representation of V indicates that defense-related functions constitute a major component of the early transcriptional response to high PAC exposure.

Because toxin-antitoxin (TA) system genes were repeatedly identified among the defense-related (COG category V) genes under both low and high PAC exposure, all differentially expressed TA system gene were compiled and summarized in Table S3. Although diverse defense-related genes were identified, TA system genes represented one of the most recurrent functional groups across PAC treatments. To further characterize the transcriptional response under severe stress, representative TA system genes differentially expressed under high PAC exposure are summarized in Table 1. High PAC exposure strongly induced multiple type II TA system genes, including members of the HicA-HicB, BrnT-BarnA, ParE/RelE-like, and MazF/PemK-like CcdA-like families (Table 1). The HicA-like toxin gene exhibited the highest induction ($log_2FC = 7.2$), whereas several paralogs within the

Preprint not peer reviewed

This preprint research paper has not been peer reviewed. Electronic copy available at: https://ssrn.com/abstract=7398765

HicA-HicB family, together with some ParE/RelE-like and StbE/RelE-like genes, were downregulated, indicating differential regulation among TA modules under high PAC stress.

Preprint not peer reviewed

This preprint research paper has not been peer reviewed. Electronic copy available at: https://ssrn.com/abstract=7398765

4. Discussion

4.1. Growth inhibition by PAC exposure

PAC exposure inhibited *Microcystis* growth by disrupting photosynthesis-related pathways (Fig. 2B and 5C). The reduction of phycocyanin (PC) levels, the primary light-harvesting pigment, was more pronounced than that chlorophyll-*a* (Fig. 2D and 2E). Moreover, the expression patterns of pigment biosynthesis genes were consistent with the observed pigment levels, suggesting transcriptional regulation of pigment production (Fig. 2E and 3A, Cluster D).

Under low PAC exposure, the doubling time increased by approximately 12h, although the culture maintained a typical growth patterns and exhibited gas vesicle formation comparable to that of the control (Fig. 2A, 2B and Table S1). Despite this relatively modest delay in cell division, cell density declined by 18.75% after 8 d and by 50.3% after 23 d, indicating that small reductions in growth rate can accumulate over time and substantially influence long-term population dynamics. In contrast, high PAC exposure severely suppressed growth, reduced gas vesicle formation, and caused visible cell wall damage within three days (Fig. 2A and B). However, the possibility cannot be excluded that the severe effects resulted not only from the higher PAC concentration but also from the concurrent decrease in pH. Previous studies have demonstrated that acidic conditions impair the growth, photosynthetic efficiency, chlorophyll-a content, and membrane integrity of *Microcystis aeruginosa* (Zhang et al. 2012, Huang et al. 2019), suggesting that low pH may have intensified the physiological deterioration observed during prolonged high PAC exposure (Fig. 2C).

Notably, cell exposed to high PAC exhibited rapid morphological alterations within 3-6 h, including changes in pigment and the appearance of dark intracellular bodies under light microscopy (Fig. 2B). Although the nature of these structures could not be determined from light microscopic observations alone, their rapid appearance suggests that PAC-induced chemical stress triggers early structural reorganization prior to extensive cell damage. Further ultrastructural analyses using transmission electron microscopy will be necessary to determine whether these changes reflect alterations in gas vesicles, intracellular storage granules, thylakoid organization, or other subcellular structures.

Preprint not peer reviewed

This preprint research paper has not been peer reviewed. Electronic copy available at: https://ssrn.com/abstract=7398765

4.2. Photosynthetic damage caused by chemical stress

Transcriptomic analysis revealed that photosynthesis was one of the earliest and most consistently affected cellular processes after PAC exposure. Both low and high PAC treatments showed coordinated downregulation of photosynthesis-related pathways (Figs. 3B and 5C), indicating that impairment of the photosynthetic apparatus represents a common response to PAC-induced chemical stress. This finding is consistent with previous studies showing that various chemical stressors suppress photosynthetic activity by disrupting pigment biosynthesis and electron transport (Sinetova and Los 2016, Moura et al. 2019, Ma et al. 2023).

Among the photosynthetic components, phycobilisome-associated genes appeared particularly sensitive to PAC exposure. Genes encoding allophycocyanin (ApcA-D) and phycocyanin/phycoerythrin proteins (CpcA-D and CpcG) were consistently downregulated (Fig. 4B), corresponding well with the marked reduction in phycocyanin content observed during cultivation (Fig. 2E). Because phycocyanin is the primary light-harvesting pigment in cyanobacteria, its decline is expected to substantially reduce light absorption and energy transfer to the photosystems (Moore et al. 2020), thereby contributing to the reduced growth observed after PAC treatment. Although chlorophyll-*a* content also decreased (Fig. 2D), the stronger reduction in phycocyanin suggests that disruption of the phycobilisome may represent an early and particularly sensitive target of PAC-induced stress.

The coordinated downregulation of photosystem I components (PsaA, PsaD, PsaE, PsaI, PsaJ, PsaK, and PsaL), together with the enrichment of genes associated with photosynthetic antenna proteins, electron transport, and thylakoid membranes (Figs. 3B and 4B), further supports the conclusion that PAC disrupts multiple components of the photosynthetic machinery. Because the thylakoid membrane is the site of photosynthetic electron transport and cellular energy conversion (Mullineaux and Liu 2020), alteration of these processes is likely to reduce photosynthetic efficiency and ultimately limit cyanobacterial proliferation.

Collectively, these findings indicate that PAC functions not only as a physical coagulant but also as a chemical stressor that directly targets the photosynthetic system. Notably, the transcriptomic responses preceded substantial reductions in cell density (Fig.

Preprint not peer reviewed

This preprint research paper has not been peer reviewed. Electronic copy available at: https://ssrn.com/abstract=7398765

2A), suggesting that disruption of light-harvesting and photosynthetic pathways represents an early molecular event during PAC exposure. This observation highlights the importance of targeting photosynthetic pigments, particularly phycobiliproteins, in future cyanobacterial bloom-control strategies. While previous management studies have primarily focused on reducing biomass or cell abundance, greater attention to pigment biosynthesis, phycobilisome assembly, and photosynthetic energy transfer may facilitate the development of more effective and selective approaches for suppressing cyanobacterial blooms.

4.3. Bacterial secretion systems and fatty acid biosynthesis in response to low PAC

Early exposure to low PAC predominantly induced genes associated with membrane remodeling, including fatty acid biosynthesis, membrane-associated secretion systems, and multidrug efflux transporters. This coordinated transcriptional response suggests that maintenance of membrane integrity represents one of the earliest adaptive responses of *M. aeruginosa* to PAC stress (Fig. 4A). Remodeling of membrane lipid composition is a common bacterial strategy for maintaining membrane fluidity, permeability, and integrity under environmental stress (Hellequin et al. 2023). Altered fatty acid biosynthesis contributes to membrane stabilization and supports the assembly and activity of membrane-associated proteins, including transporters and secretion systems (Zhang and Rock 2008, Sohlenkamp and Geiger 2016). Consistent with this response, genes encoding components of the type I secretion system (HlyB/HlyD), type II secretion system (GspH), and the AcrAB multidrug efflux system were also induced. Because these transport systems are embedded within the cytoplasmic membrane, membrane remodeling likely provides the structural basis for efficient secretion and efflux under chemical stress.

In summary, these observations support a model in which membrane remodeling constitutes the primary adaptive response to low PAC exposure, enabling activation of secretion systems and multidrug efflux transporters that may reduce intracellular accumulation of PAC before irreversible cellular damage occurs.

4.4. Toxin–antitoxin systems as an early stress response to high PAC

Preprint not peer reviewed

This preprint research paper has not been peer reviewed. Electronic copy available at: https://ssrn.com/abstract=7398765

TA systems are widely distributed genetic modules that play important roles in bacterial stress adaptation by regulating growth, persistence, and dormancy rather than functioning solely as cell death mechanisms (Frees et al. 2004, Page and Peti 2016, Singh et al. 2021). In the present study, several type II TA modules, including the HicA-HicB, BrnT-BrnA, ParE/RelE, MazF/PemK, and MqsA families, were differentially expressed following high PAC exposure. Among these, the HicA-HicB family exhibited the strongest transcriptional response, whereas additional TA families were also induced, suggesting that severe PAC stress activates multiple regulatory pathways involved in growth arrest and stress adaptation rather than a single conserved response (Table 1).

Interestingly, most HicA-HicB paralogs were downregulated or exhibited contrasting transcriptional responses, whereas one HicA paralog was markedly upregulated under high PAC exposure and several others responded under low PAC conditions. These distinct expression patterns suggest that HicA-HicB paralogs are not functionally redundant but instead may be differentially regulated according to the nature and intensity of environmental stress. Given that HicA functions as an RNase that regulates RNA stability and translation through selective RNA cleavage (Jørgensen et al. 2009, Thomet et al. 2019), the differential expression of HicA paralogs raises the possibility that individual paralogs regulate distinct RNA targets and metabolic programs during stress adaptation.

The downstream regulatory networks controlled by individual TA systems during PAC stress remain largely unknown. Future studies should therefore identify the RNA targets and regulatory networks associated with stress-responsive TA modules using targeted genetic manipulation together with transcriptomic, translatomic (e.g., ribosome profiling), and metabolomic analyses. Integrating these approaches will help reveal how environmental stress signals are translated into coordinated metabolic reprogramming through RNA-mediated regulatory mechanisms. Our findings provide evidence that RNA-level regulation represents an important component of the early stress response in cyanobacteria and highlight RNA-mediated metabolic regulation as a promising direction for future studies of cyanobacterial stress adaptation. If these regulatory mechanisms are experimentally validated, they could provide a conceptual foundation for developing RNA-based strategies to manipulate stress responses for diverse biological and biotechnological applications.

Preprint not peer reviewed

This preprint research paper has not been peer reviewed. Electronic copy available at: https://ssrn.com/abstract=7398765

5. Conclusion

Residual *Microcystis* cells that persist following chemical coagulant treatment remain a key challenge in bloom management, as they may survive, recover, and contribute to bloom recurrence. While polyaluminum chloride (PAC) is widely used for effective biomass removal, this study reveals its sublethal effects under low-dose exposure and underscores the adaptive potential of *Microcystis aeruginosa*. Our findings demonstrate that PAC exposure disrupts photosynthetic pathways, particularly by downregulating genes involved in the photosystem II antenna complex and phycobilisome structure, leading to reduced phycocyanin pigment production. Transcriptomic analysis further revealed that low PAC exposure induced membrane remodeling, bacterial secretion systems, and multidrug efflux transporters, suggesting activation of early adaptive defense mechanisms. In contrast, high PAC exposure triggered coordinated transcriptional responses involving multiple toxin-antitoxin (TA) systems, indicating that severe chemical stress is accompanied by extensive regulatory reprogramming rather than a single conserved stress response. These molecular responses provide new insight into the hierarchical stress adaptation strategy of *M. aeruginosa*, in which photosynthetic inhibition, membrane remodeling, and activation of RNA-associated regulatory systems together contribute to physiological adaptation under chemical stress. This integrated response suggests that environmental stress is not mediated by isolated pathways but instead involves coordinated metabolic reprogramming across multiple cellular processes. Thus, our findings provide a broader perspective on how cyanobacteria respond to environmental stress at the molecular level. The transcriptomic responses observed in this study suggest that RNA-mediated regulatory mechanisms may represent a central layer linking environmental stress perception with metabolic reprogramming and physiological adaptation. Deciphering these regulatory networks will advance our understanding of bacterial stress biology and establish a foundation for future studies exploring RNA-mediated regulation as a fundamental mechanism coordinating environmental stress responses in cyanobacteria and other photosynthetic microorganisms.

Preprint not peer reviewed

This preprint research paper has not been peer reviewed. Electronic copy available at: https://ssrn.com/abstract=7398765

CRediT authorship contribution statement

Eun-jeong Kim: Conceptualization, Data curation, Formal analysis, Methodology, Visualization, Funding acquisition, Writing – Original Draft and Reviewing & Editing. **Yeon-jeong Park**: Data curation, Formal analysis, Methodology, Writing – Original Draft and Reviewing & Editing. **Jae Hak Lee**: Data curation, Methodology. **Heesuk Lee**: Data curation, Funding acquisition, Methodology. **Han Soon Kim**: Conceptualization, Data curation.

Declaration of competing interest

The authors declare that they have no known competing financial interests or personal relationships that could have appeared to influence the work reported in this paper.

Data availability

Raw reads corresponding to transcriptome analyses have been deposited in the NCBI Sequence Read Archive under the BioProject identification number PRJNA1142213.

Acknowledgements

The authors gratefully acknowledge Dr. Chi-Yong Ahn, Cell factory Research Center, KRIBB, Daejeon 34350, Korea, for generously providing the *Microcystis aeruginosa* KW strain. This work was supported by the National Research Foundation of Korea (NRF) grant funded by the Korea government (MSIT) [RS-2026-25484166]; National Research Council of Science & Technology (NST) grant by the Korea government (MSIT) [CAP-18-07-KICT].

Appendix A. Supplementary data

Supplementary data to this article can be found online at https://doi.org/00000000000.

Preprint not peer reviewed

This preprint research paper has not been peer reviewed. Electronic copy available at: https://ssrn.com/abstract=7398765

References

Arruda, R. S., N. P. Noyma, L. de Magalhaes, M. C. B. Mesquita, E. C. de Almeida, E. Pinto, M. Lurling, and M. M. Marinho. 2021. 'Floc and Sink' Technique Removes Cyanobacteria and Microcystins from Tropical Reservoir Water. Toxins (Basel) **13**.

Bennett, A., and L. Bogorad. 1973. Complementary chromatic adaptation in a filamentous blue-green alga. The Journal of cell biology **58**:419.

Casamassimi, A., and A. Ciccodicola. 2019. Transcriptional Regulation: Molecules, Involved Mechanisms, and Misregulation. Int J Mol Sci **20**.

Du, C., W. Sang, C. Xu, Z. Jiang, J. Wang, Y. Fang, C. Zhu, J. Wizi, M. A. Akram, L. Ni, and S. Li. 2023. Integrated transcriptomic and metabolomic analysis of *Microcystis aeruginosa* exposed to artemisinin sustained-release microspheres. J Hazard Mater **443**:130114.

EPA. 2022. Polyaluminum Chloride Supply Chain Profile. EPA.

Frees, D., A. Chastanet, S. Qazi, K. Sørensen, P. Hill, T. Msadek, and H. Ingmer. 2004. Clp ATPases are required for stress tolerance, intracellular replication and biofilm formation in Staphylococcus aureus. Molecular Microbiology **54**:1445-1462.

Galperin, M. Y., K. S. Makarova, Y. I. Wolf, and E. V. Koonin. 2015. Expanded microbial genome coverage and improved protein family annotation in the COG database. Nucleic Acids Res **43**:D261-269.

Glibert, P. M. 2020. Harmful algae at the complex nexus of eutrophication and climate change. Harmful Algae **91**:101583.

Harke, M. J., D. L. Berry, J. W. Ammerman, and C. J. Gobler. 2012. Molecular Response of the Bloom-Forming Cyanobacterium, *Microcystis aeruginosa*, to Phosphorus Limitation. Microbial Ecology **63**:188-198.

Harke, M. J., and C. J. Gobler. 2013. Global transcriptional responses of the toxic cyanobacterium, *Microcystis aeruginosa*, to nitrogen stress, phosphorus stress, and growth on organic matter. PLoS One **8**:e69834.

Harke, M. J., and C. J. Gobler. 2015. Daily transcriptome changes reveal the role of nitrogen in controlling microcystin synthesis and nutrient transport in the toxic cyanobacterium, *Microcystis aeruginosa*. BMC Genomics **16**:1068.

Hellequin, E., S. Collin, M. Seder-Colomina, P. Véquaud, C. Anquetil, A. Kish, and A. Huguet. 2023. Membrane lipid adaptation of soil Bacteroidetes isolates to temperature and pH. Front Microbiol **14**:1032032.

Hong, Y., J. J. Huang, and H. Y. Hu. 2009. Effects of a novel allelochemical ethyl 2-methyl acetoacetate (EMA) on the ultrastructure and pigment composition of cyanobacterium *Microcystis aeruginosa*. Bull Environ Contam Toxicol **83**:502-508.

Huang, Y., H. Pan, H. Liu, Y. Xi, and D. Ren. 2019. Characteristics of growth and microcystin production of *Microcystis aeruginosa* exposed to low concentrations of naphthalene and phenanthrene under different pH values. Toxicon **169**:103-108.

Jeong, H., S.-J. Chun, A. Srivastava, Y. Cui, S.-R. Ko, H.-M. Oh, and C.-Y. Ahn. 2018. Genome Sequences of Two Cyanobacterial Strains, Toxic Green Microcystis aeruginosa KW (KCTC 18162P) and Nontoxic Brown Microcystis sp. Strain MC19, under Xenic Culture Conditions. Genome Announcements **6**:e00378-00318.

Jørgensen, M. G., D. P. Pandey, M. Jaskolska, and K. Gerdes. 2009. HicA of Escherichia coli defines a novel family of translation-independent mRNA interferases in bacteria and archaea. J Bacteriol **191**:1191-1199.

This preprint research paper has not been peer reviewed. Electronic copy available at: https://ssrn.com/abstract=7398765

Kang, J., Y. S. Kwak, E.-j. Kim, Y. Gwon, H. G. Choi, and S.-i. Eyun. 2024. Transcriptome and functional analyses of phenotypic plasticity in sea grape Caulerpa okamurae. Physiologia Plantarum **176**:e14339.

Kim, E. J., H. Doh, J. Yang, and S. I. Eyun. 2024. The occurrence of positive selection on BicA transporter of *Microcystis aeruginosa*. Ecotoxicol Environ Saf **283**:116795.

Kurniawan, S. B., M. F. Imron, C. E. N. C. E. Chik, A. A. Owodunni, A. Ahmad, M. M. Alnawajha, N. F. M. Rahim, N. S. M. Said, S. R. S. Abdullah, N. A. Kasan, S. Ismail, A. R. Othman, and H. A. Hasan. 2022. What compound inside biocoagulants/bioflocculants is contributing the most to the coagulation and flocculation processes? Science of The Total Environment **806**:150902.

Lürling, M., M. Mucci, and G. Waajen. 2020. Removal of Positively Buoyant Planktothrix rubescens in Lake Restoration. Toxins (Basel) **12**.

Ma, Y., F. Yan, L. An, W. Shen, T. Tang, Z. Li, and R. Dai. 2023. Transcriptome analysis of changes in M. aeruginosa growth and microcystin production under low concentrations of ethinyl estradiol. Sci Total Environ **859**:160226.

MacQueen, J. 1967. Some methods for classification and analysis of multivariate observations. Pages 281-297 *in* Proceedings of the fifth Berkeley symposium on mathematical statistics and probability. Oakland, CA, USA.

Mehdizadeh, S., M. Yasukawa, T. Suzuki, and M. Higa. 2020. Reverse electrodialysis for power generation using seawater/municipal wastewater: Effect of coagulation pretreatment. Desalination **481**.

Miranda, M., N. Noyma, F. S. Pacheco, L. de Magalhães, E. Pinto, S. Santos, M. F. A. Soares, V. L. Huszar, M. Lürling, and M. M. Marinho. 2017. The efficiency of combined coagulant and ballast to remove harmful cyanobacterial blooms in a tropical shallow system. Harmful Algae **65**:27-39.

Moore, K. A., S. Altus, J. W. Tay, J. B. Meehl, E. B. Johnson, D. M. Bortz, and J. C. Cameron. 2020. Mechanical regulation of photosynthesis in cyanobacteria. Nat Microbiol **5**:757-767.

Morimoto, D., S. Kimura, Y. Sako, and T. Yoshida. 2018. Transcriptome Analysis of a Bloom-Forming Cyanobacterium *Microcystis aeruginosa* during Ma-LMM01 Phage Infection. Front. Microbiol. **9**:2.

Moura, K. A. F., C. Lizieri, M. Wittig Franco, M. Vaz, W. L. Araújo, P. Convey, and F. A. R. Barbosa. 2019. Physiological and thylakoid ultrastructural changes in cyanobacteria in response to toxic manganese concentrations. Ecotoxicology **28**:1009-1021.

Mullineaux, C. W., and L. N. Liu. 2020. Membrane Dynamics in Phototrophic Bacteria. Annu Rev Microbiol **74**:633-654.

Najm, I., C. Tate, and D. Selby. 1998. Optimizing enhanced coagulation with PAC: A case study. Journal AWWA **90**:88-95.

Ndikubwimana, T., X. Zeng, T. Murwanashyaka, E. Manirafasha, N. He, W. Shao, and Y. Lu. 2016. Harvesting of freshwater microalgae with microbial bioflocculant: a pilot-scale study. Biotechnology for Biofuels **9**:47.

Page, R., and W. Peti. 2016. Toxin-antitoxin systems in bacterial growth arrest and persistence. Nat Chem Biol **12**:208-214.

Rice, E. W., L. Bridgewater, A. P. H. Association, A. W. W. Association, and W. E. Federation. 2012. Standard Methods for the Examination of Water and Wastewater. American Public Health Association.

Sinetova, M. A., and D. A. Los. 2016. Lessons from cyanobacterial transcriptomics: Universal genes and triggers of stress responses. Molecular Biology **50**:606-614.

Singh, G., M. Yadav, C. Ghosh, and J. S. Rathore. 2021. Bacterial toxin-antitoxin modules:

This preprint research paper has not been peer reviewed. Electronic copy available at: https://ssrn.com/abstract=7398765

classification, functions, and association with persistence. Curr Res Microb Sci **2**:100047.
Sohlenkamp, C., and O. Geiger. 2016. Bacterial membrane lipids: diversity in structures and pathways. FEMS Microbiol Rev **40**:133-159.
Stark, R., M. Grzelak, and J. Hadfield. 2019. RNA sequencing: the teenage years. Nat Rev Genet **20**:631-656.
Tang, X., L. E. Krausfeldt, K. Shao, G. R. LeCleir, J. M. A. Stough, G. Gao, G. L. Boyer, Y. Zhang, H. W. Paerl, B. Qin, and S. W. Wilhelm. 2018. Seasonal Gene Expression and the Ecophysiological Implications of Toxic *Microcystis aeruginosa* Blooms in Lake Taihu. Environ Sci Technol **52**:11049-11059.
Thomet, M., A. Trautwetter, G. Ermel, and C. Blanco. 2019. Characterization of HicAB toxin-antitoxin module of Sinorhizobium meliloti. BMC Microbiol **19**:10.
Wang, Z., M. Gerstein, and M. Snyder. 2009. RNA-Seq: a revolutionary tool for transcriptomics. Nat Rev Genet **10**:57-63.
Wilhelm Steven, W., S. Bullerjahn George, and R. M. L. McKay. 2020. The Complicated and Confusing Ecology of *Microcystis* Blooms. mBio **11**:10.1128/mbio.00529-00520.
Yan, X., X. Xu, M. Wang, G. Wang, S. Wu, Z. Li, H. Sun, A. Shi, and Y. Yang. 2017. Climate warming and cyanobacteria blooms: Looks at their relationships from a new perspective. Water Research **125**:449-457.
Yang, M., Z. Fan, Y. Xie, L. Fang, X. Wang, Y. Yuan, and R. Li. 2020. Transcriptome analysis of the effect of bisphenol A exposure on the growth, photosynthetic activity and risk of microcystin-LR release by *Microcystis aeruginosa*. J Hazard Mater **397**:122746.
Yang, X., Y. Bi, X. Ma, W. Dong, X. Wang, and S. Wang. 2022. Transcriptomic analysis dissects the regulatory strategy of toxic cyanobacterium *Microcystis aeruginosa* under differential nitrogen forms. Journal of Hazardous Materials **428**:128276.
Yang, Y., Q. Li, S. Yan, P. Zhang, H. Zhang, X. Kong, H. Wang, L.-A. Hansson, S. Xie, J. Xu, and H. Wang. 2024. Eutrophication promotes resource use efficiency and toxin production of *Microcystis* in a future climate warming scenario. Environmental Research **263**:120219.
Zhang, H., L. Li, S. Cheng, C. Li, F. Liu, P. Wang, L. Sun, J. Huang, W. Zhang, and X. Zhang. 2023. Enhanced Microcystis Aeruginosa removal and novel flocculation mechanisms using a novel continuous co-coagulation flotation (CCF). Science of The Total Environment **857**:159532.
Zhang, M., Y. Wang, Y. Wang, M. Li, D. Zhang, Z. Qiang, and X. Pan. 2019. Efficient elimination and re-growth inhibition of harmful bloom-forming cyanobacteria using surface-functionalized microbubbles. Water Research **161**:473-485.
Zhang, Y., X. Li, J. Liang, Y. Luo, N. Tang, S. Ye, Z. Zhu, W. Xing, J. Guo, and H. Zhang. 2022. Microcystis aeruginosa's exposure to an antagonism of nanoplastics and MWCNTs: The disorders in cellular and metabolic processes. Chemosphere **288**:132516.
Zhang, Y., C. Y. Tang, and G. Li. 2012. The role of hydrodynamic conditions and pH on algal-rich water fouling of ultrafiltration. Water Res **46**:4783-4789.
Zhang, Y. M., and C. O. Rock. 2008. Membrane lipid homeostasis in bacteria. Nat Rev Microbiol **6**:222-233.

Preprint not peer reviewed

This preprint research paper has not been peer reviewed. Electronic copy available at: https://ssrn.com/abstract=7398765

Figures

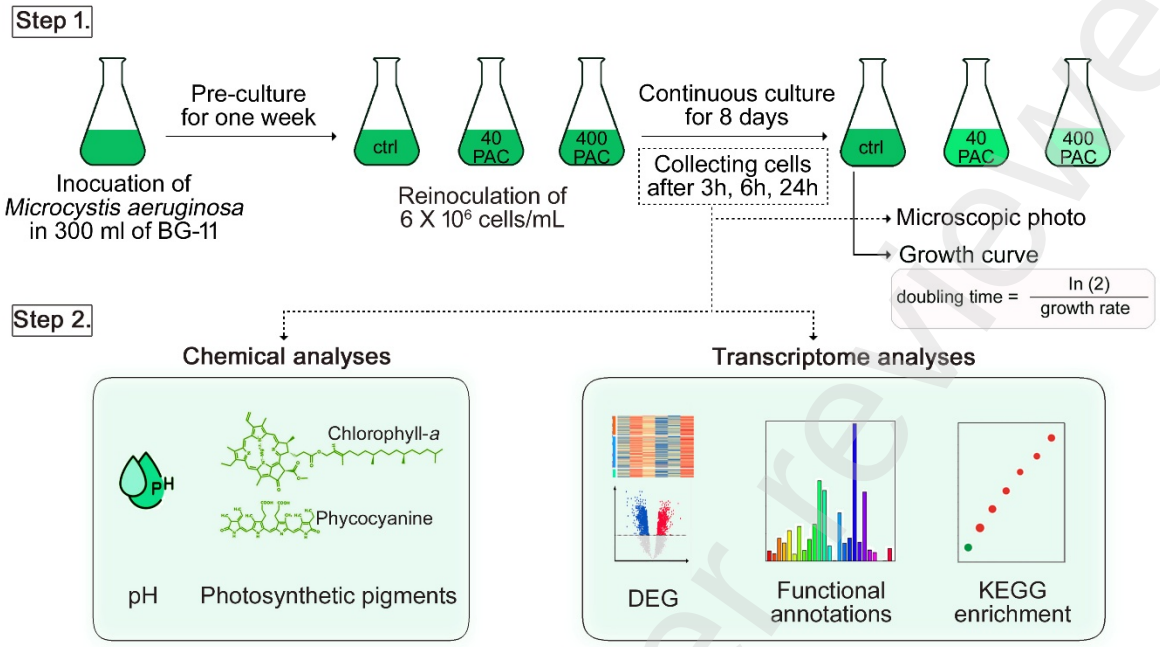


Fig. 1. Schematic diagram of the experimental process. Step 1: Cell culture and PAC treatment. Step 2: Chemical and transcriptome analyses.

Preprint not peer reviewed

This preprint research paper has not been peer reviewed. Electronic copy available at: https://ssrn.com/abstract=7398765

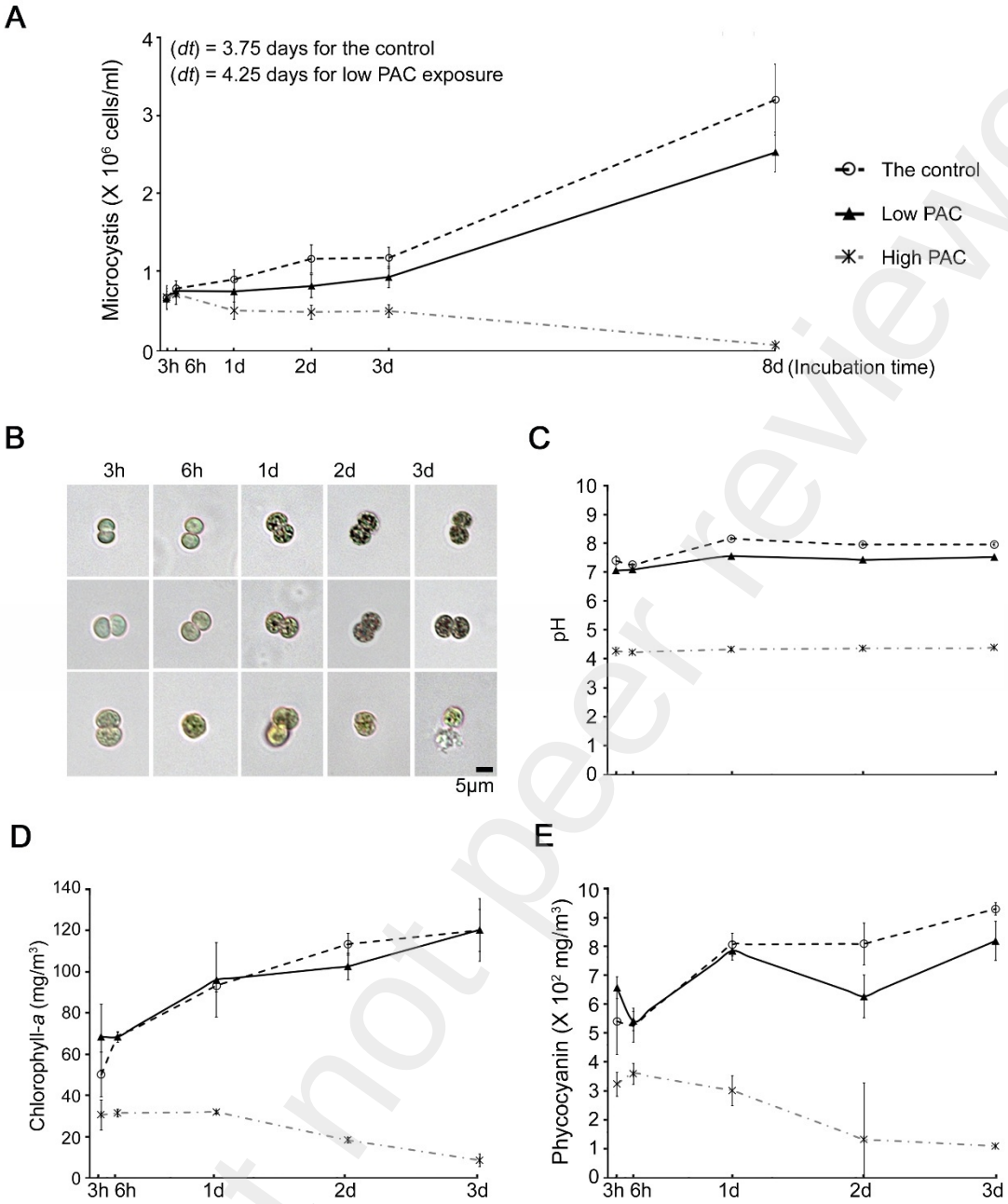


Fig. 2. Growth curves and photosynthetic pigment analysis of *Microcystis aeruginosa*. A) Growth curves for the control, low PAC exposure, and high PAC exposure groups over eight days. The doubling time (*dt*) was calculated to be 3.75 days and 4.25 days for the control and low PAC treatment, respectively. B) Microscopic images showing phenotypic changes to the *Microcystis* cells. C–E) Chemical analysis of pH, chlorophyll-*a*, and phycocyanin over three days.

This preprint research paper has not been peer reviewed. Electronic copy available at: https://ssrn.com/abstract=7398765

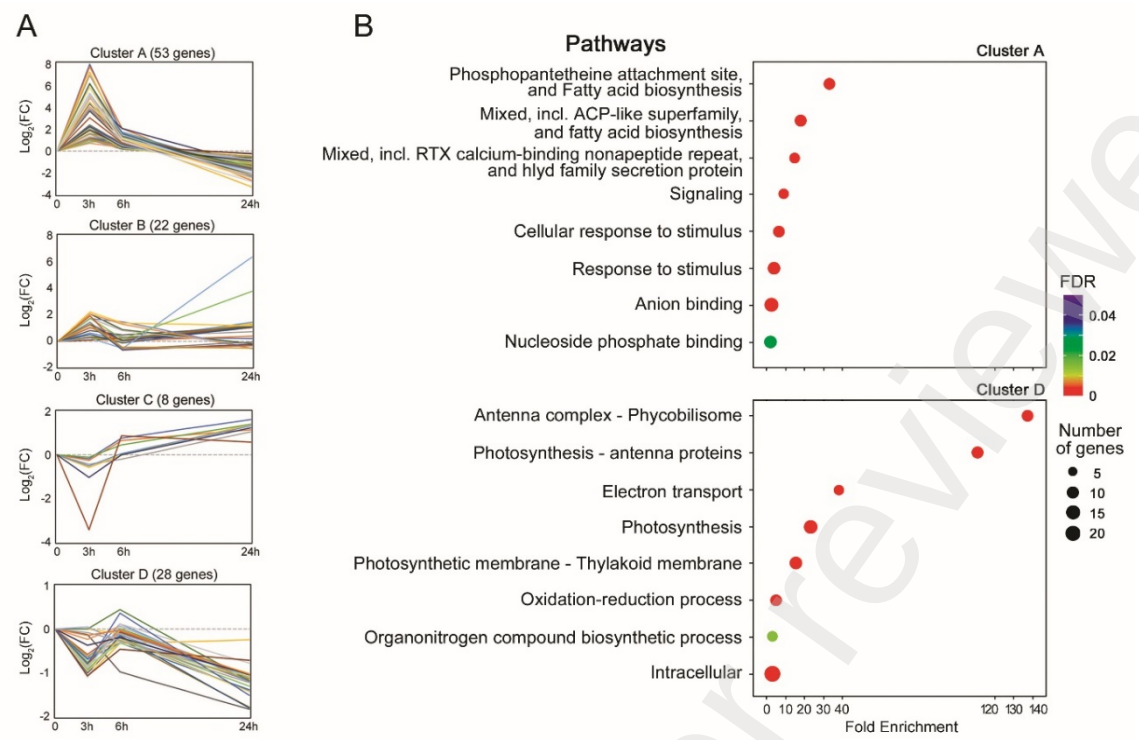


Fig. 3. Transcriptomic dynamics and pathway enrichment analysis in response to low PAC exposure in *M. aeruginosa*. A) Cluster analysis of DEGs using the *k*-means algorithm. Only genes with a false discovery rate (FDR) *p*-value of less than 0.05 and a $\log_2$ fold change of (fc) ≥ 1 were included in the analysis. On the *x*-axis, each time point represents a comparison of the low PAC treatment vs. the control, while the $\log_2$ fold change in gene expression levels is presented on the *y*-axis. B) Functional enrichment analysis associated with Clusters A and D, which contain 53 and 28 genes, respectively. The cut-off criteria include a false discovery ratio (FDR) threshold of less than 0.05 and more than five genes.

Preprint not peer reviewed

This preprint research paper has not been peer reviewed. Electronic copy available at: https://ssrn.com/abstract=7398765

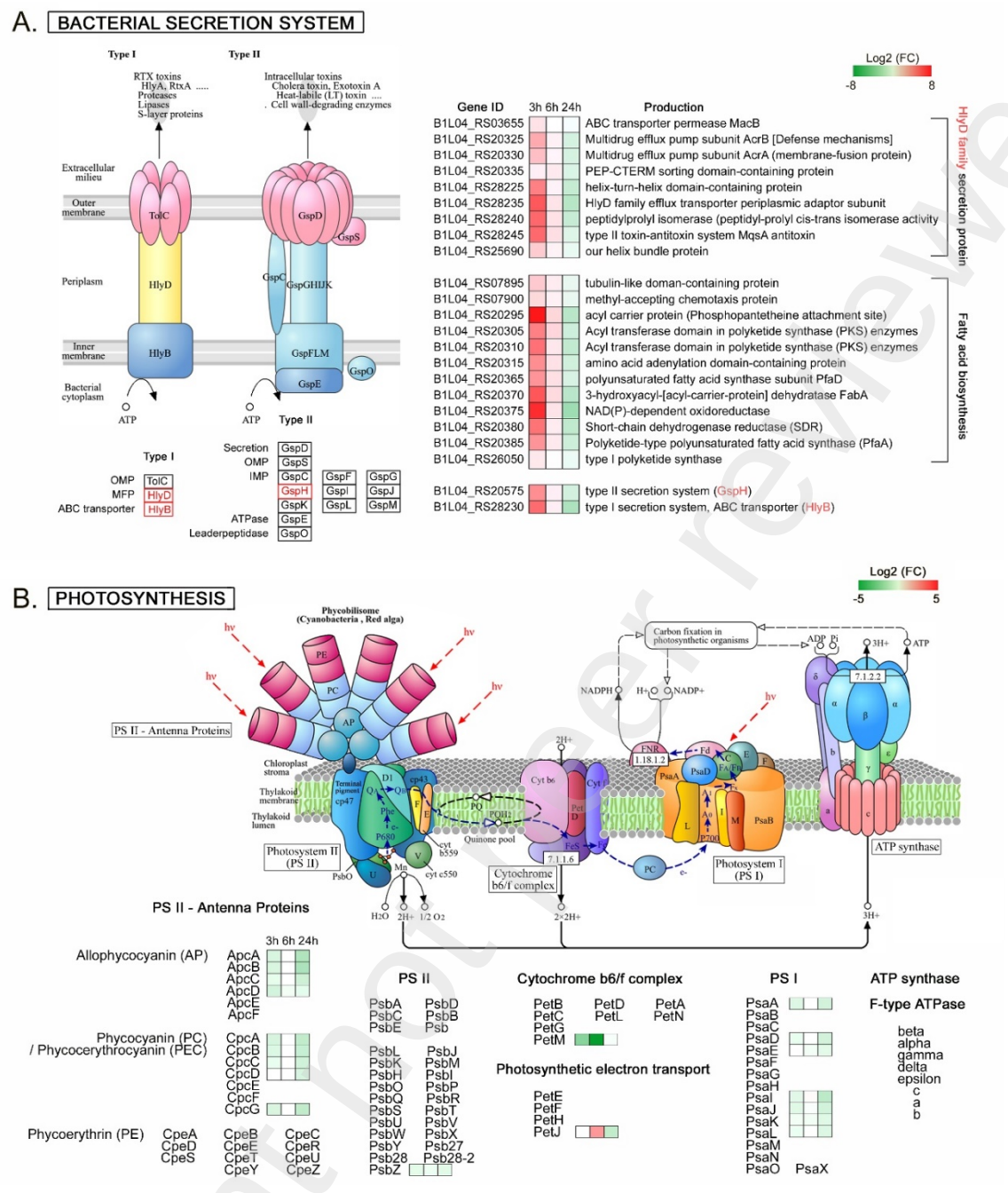


Fig. 4. KEGG pathway modules for bacterial secretion systems and photosynthesis. The KEGG pathway map for bacterial type I and type II secretion systems is derived from map03070, and photosynthesis and photosynthesis antenna proteins are derived from map00195 and map00196, respectively.

This preprint research paper has not been peer reviewed. Electronic copy available at: https://ssrn.com/abstract=7398765

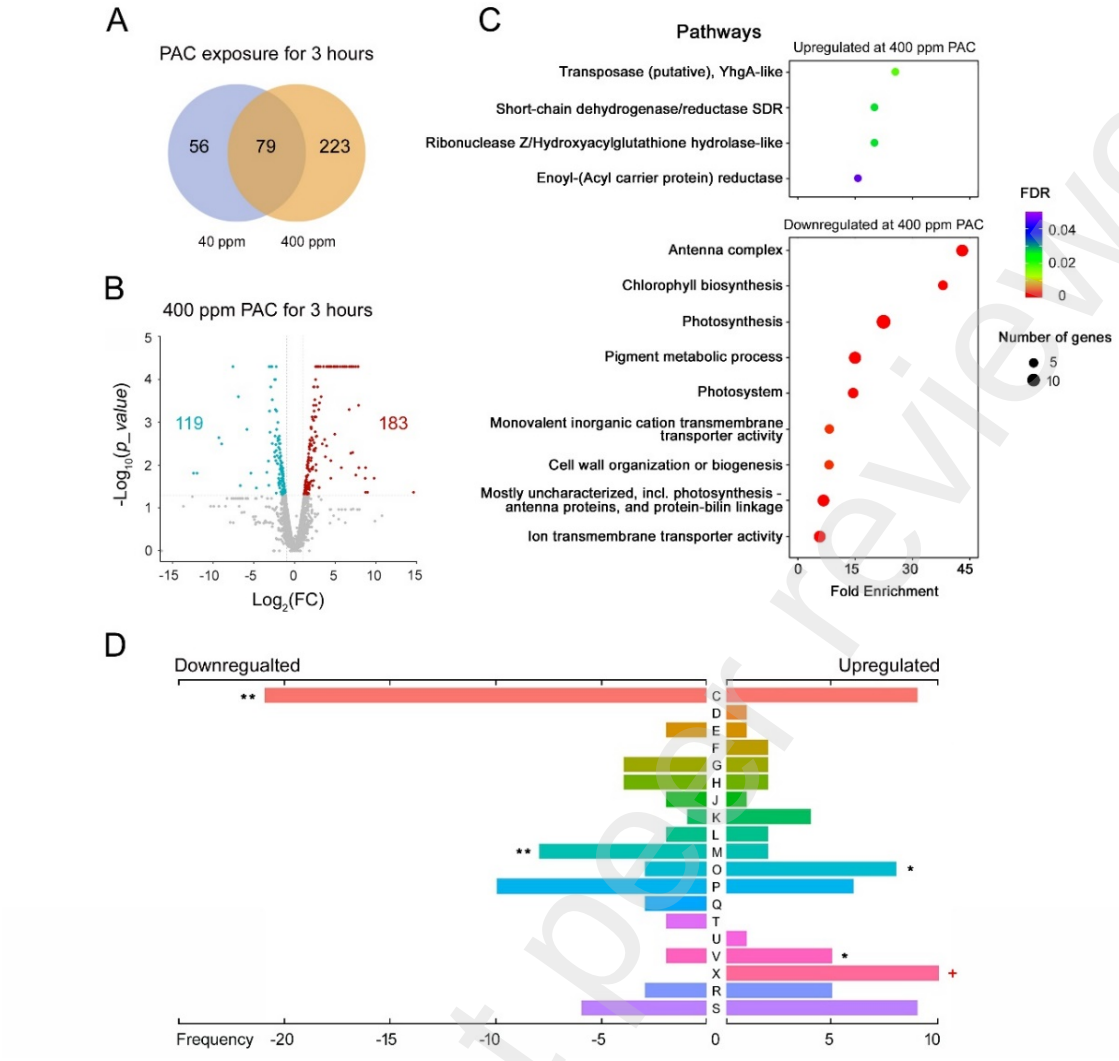


Fig. 5. Differential expression analysis under high PAC exposure for 3 h. A) Venn diagram of unique and overlapping DEGs for low and high PAC exposure. B) Volcano plot depicting upregulated genes in red and downregulated genes in blue. The numbers for each color represent only DEGs with a false discovery rate (FDR) p-value of < 0.05 and a $\log_2$ fold change of (fc) ≥ 1. C) Gene enrichment under high PAC exposure. The cut-off criteria include an FDR threshold of less than 0.05. D) Functional classification of clusters of orthologous groups (COGs). The plus symbol (+) indicates unique upregulated genes with a frequency greater than 5. Both upregulated and downregulated classes with a frequency greater than 5 and a frequency difference of more than 2.5 times are marked with * and **, respectively. COG classes; C: Energy production and conversion, D: Cell cycle control and mitosis, E: Amino acid metabolism and transport, F: Nucleotide metabolism and transport, G: Carbohydrate metabolism and transport, H: Coenzyme metabolism, J: Translation, K: Transcription, L: Replication and repair, M: Cell wall biogenesis, O: Post-translational modification, protein turnover, and chaperone functions, P: Inorganic ion transport and metabolism, Q: Secondary structure, T: Signal transduction, U: Intracellular trafficking and secretion, V: Defense mechanisms, X: Mobilome, R: General functional prediction only, S: Function unknown.

This preprint research paper has not been peer reviewed. Electronic copy available at: https://ssrn.com/abstract=7398765

Table 1. Eight superfamilies of type II toxin-antitoxin (TA) systems significantly expressed in response to high PAC exposure. Protein ID for NCBI.

	Gene ID (Protein ID)	Log_2 (FC)
BrnT-BrnA TA system		
BrnA-like antitoxin	B1L04_RS17595 (WP_002738362.1)	**7.0**
BrnT-like toxin	B1L04_RS02815 (WP_079205719.1)	**1.5**
	B1L04_RS22050 (WP_024970787.1)	**1.1**
HicA-HicB TA systems		
HicB-like antitoxin	B1L04_RS03280 (WP_002749012.1)	**1.5**
	B1L04_RS08295 (WP_016515139.1)	-1.0
	B1L04_RS11115 (WP_002776494.1)	-1.3
	B1L04_RS07850 (WP_002732327.1)	-3.4
HicA-like toxin	B1L04_RS26210 (WP_002732521.1)	**7.2**
	B1L04_RS05540 (WP_002782277.1)	-1.0
	B1L04_RS10715 (WP_079207302.1)	-1.0
	B1L04_RS18535 (WP_008199366.1)	-1.9
	B1L04_RS05500 (WP_079206058.1)	-3.8
	B1L04_RS02395 (WP_012267861.1)	-4.8
	B1L04_RS02520 (WP_012267861.1)	-4.8
	B1L04_RS07845 (WP_079206480.1)	-4.8
ParE/RelE-like toxin		
	B1L04_RS18630 (WP_002798430.1)	**2.1**
	B1L04_RS02085 (WP_002734670.1)	**1.3**
	B1L04_RS23490 (WP_043997021.1)	**1.0**
	B1L04_RS21730 (WP_002799477.1)	-1.4
	B1L04_RS02070 (WP_239698146.1)	-1.7
	B1L04_RS01325 (WP_249267815.1)	-2.9
StbE/RelE-like toxin		
	B1L04_RS05575 (WP_002782273.1)	-1.1
	B1L04_RS03270 (WP_079205801.1)	-1.2
	B1L04_RS02275 (WP_061432389.1)	-3.6
MazF/PemK-like toxin		
	B1L04_RS19215 (WP_079209012.1)	**1.4**
	B1L04_RS07505 (WP_079206402.1)	**1.4**
MqsA-like antitoxin		
	B1L04_RS28245 (WP_079210232.1)	**5.4**
CcdA-like antitoxin		
	B1L04_RS03415 (WP_002732463.1)	**1.8**
prevent-host-death-like antitoxin		
	B1L04_RS02295 (WP_002796331.1)	-2.5

Preprint not peer reviewed

This preprint research paper has not been peer reviewed. Electronic copy available at: https://ssrn.com/abstract=7398765